Numerical Methods in Civil Engineering, 10-2 (2025) 102-117

Numerical Methods in Civil Engineering

Parametric Numerical Study and Behavioral Modeling of a Hybrid Steel–SMA Axial Damper

Behrouz Asgarian*, Majid Amir Ahmadi, Ali Jalaeefar*****

ARTICLE INFO

RESEARCH PAPER

Article history:
Received:
January 2024
Revised:
December 2025
Accepted:
February 2026

Keywords:
Hybrid Damper, SMA Bars, Steel Bars, Effective Parameters, Analytical Behavioural Model.

Abstract:

This paper addresses the major parameters affecting the behavior of hybrid dampers consisting of shape-memory alloy (SMA) and steel materials, subjected to cyclic loadings, and a numerical behavioral model is proposed. The hybrid damper investigated in this study was originally developed and experimentally examined in previous research, and the present work aims to extend those studies through numerical analysis. For this purpose, first, the hybrid damper was numerically modeled and verified using a code written in MATLAB software. Then, the behavior of the damper under cyclic loadings was investigated by altering the main parameters, such as length and diameter of the inelastic part, length of the elastic part, number of bars, and steel grade through a systematic numerical parametric study. In the next step, a numerical hysteretic behavioral model was proposed for the damper by which the nonlinear response could be simulated. Based on the obtained results, as the diameter and length of the inelastic part as well as the number of the steel bars increase, the energy dissipation capacity of the damper improves, and also the contribution of the SMA bars to the self-centering behavior is enhanced. However, increasing the length of the elastic part of the steel and SMA bars reduces the energy dissipation and residual displacement values, which ultimately does not enhance the dampers' behavior. Finally, the developed behavioral model was verified using available experimental results. The results revealed that the proposed model is sufficiently accurate for numerically simulating the behavior and performance of the hybrid damper composed of steel and SMA bars under cyclic displacement-controlled loading.

1. Introduction

The passive control methods to protect the structures against earthquakes are considered suitable alternatives for traditional methods these days. These systems are designed to absorb and dissipate seismic actions by specific mechanisms. The passive control is implemented by installing passive dampers in the pre-determined locations of the structure. The dampers are mainly responsible for absorbing the input seismic energy and reducing the induced displacements to protect the structural and non-structural components of the structures [1, 2].

Skinner and Kelly [3, 4] are the pioneers of studying the steel dampers that were introduced for seismic energy dissipation in structural systems. Kafi et al. [5] utilized a steel ring in the concentric braces, which was supposed to function as a structural fuse. Results of the experimental and numerical analyses indicated that the use of the steel rings could be practical and efficient. Bracone et al. [6] introduced a self-centering damper, which was composed of three main parts, namely steel skeleton, energy dissipater element and pre-tensioned components. The results showed acceptable performance of this damper, as it was able to properly return to its pre-deformed state with no residual displacements. Motamedi et al. and Peng et al. [7, 8] investigated the hysteretic curve of a steel ring functioning as the structural fuse. Based on the obtained results, they concluded that the

** Professor, Department of civil engineering, K.N. Toosi University of Technology, Tehran, Iran.*
*** MSc, Department of civil engineering, K.N. Toosi University of Technology, Tehran, Iran*
**** Corresponding author:Department of Civil Engineering, NT.C., Islamic Azad University, Tehran, Iran - Email: ali_jalaeefar@yahoo.com, alijalaeefar@iau.ac.ir*

https://doi.org/10.61882/NMCE.2401.1046

ring has an appropriate performance in ductility and energy absorption. Gao et al. [9] developed a novel bracing system made of SMA. In this system, an SMA ring was located at the conjunction of the concentric braces. It was observed that the use of this system could significantly improve the ductility and energy dissipation capacity [9]. Andalib et al. [10] carried out a numerical study on ductility and energy absorption capacity of the steel rings with end plates. For this purpose, the rings were comprised of two half-rings. Peng et al. [11] investigated the seismic behavior of the steel frames equipped with chevron bracing including a steel ring. The results indicated that theuse of the steel ring, could enhance the ductility and energy absorption capacity of the system.

On the other hand, after introducing the SMAs, many studies were conducted to utilize them in the dampers. One of the outstanding characteristics of these alloys that has led to widespread use of them in the structural engineering industry, is associated with their ability to return to the pre-deformed shape [12]. In the following, some of the research conducted in this field, are reviewed accordingly.

Zhang et al. [13] developed a friction damper reinforce with the SMA wires. In this study, in addition to investigating the tensile behavior of the SMA wires, the damper was subjected to cyclic loading. The results indicated that compared to the case when buckling-restrained braces (BRBs) are employed, the use of this innovative damper results in smaller residual displacements. Karavasilis et al. [14] introduced a novel self-centering damper, consisting of a visco-elastic damper and a self-centering device combined in series. The damper was composed of two steel elements and two groups of SMA wires. The SMA wires were positioned such that once the steel elements started moving, the SMA wires were subjected to tension forces. In this case, the energy would be dissipated by the friction between the steel elements. It was found that the use of this damper could reduce the residual displacements and enhance the energy dissipation capacity. Ozebolto et al. [15] proposed a self-centering damper, consisting of three parts, namely a frictional segment, a physio-electronic actuator, and SMA wires. Based on the results, it was concluded that in the frame without the damper, energy is dissipated because of the plastic deformation of the frame but when the damper is installed, a major portion of the energy is absorbed by the damper that decreases the plastic displacements and consequently, less damage is induced to the structure [15]. To improve the energy-dissipating capacity of the SMA dampers, Qiu et al. [16] proposed to utilize the SMA elements with steel dampers. In this novel steel-SMA damper, the steel dampers are majorly responsible for absorbing the input energy, whereas the SMA wires have to return the system to the initial state. Mirzaei et al. [17] developed smart hybrid dampers equipped with SMA plates, friction pads and polyurethane springs. This innovative damper was proposed to minimize structural damage and reduce residual displacements in concentrically-braced frames (CBFs). Inspired by the complementary behavior of steel and SMA materials, Jalaeefar and Asgarian [18–21] proposed a hybrid axial damper composed of structural steel and nickel–titanium SMA bars. This damper was experimentally and numerically investigated in previous studies, and the results demonstrated stable hysteretic behavior, significant energy dissipation, and effective self-centering capability. Despite these promising results, a detailed numerical parametric investigation addressing the influence of key geometric and material parameters, as well as a unified numerical behavioral model suitable for structural analysis applications, has not been fully developed.

Accordingly, the present study aims to extend the previous experimental research by conducting a comprehensive numerical parametric study on the hybrid steel–SMA axial damper. The effects of key parameters—including the diameter and length of the inelastic part, length of the elastic part, number of bars, and steel grade—are systematically evaluated under cyclic displacement-controlled loading. Based on the observed numerical hysteretic responses, a numerical behavioral model is subsequently developed to represent the damper response in a simplified yet accurate form, enabling efficient implementation in numerical seismic analyses of structures.

2. Numerical Modeling

2.1 Introduction of the proposed Hybrid Damper

In this paper, a parametric study is conducted on the self-centering damper introduced by Jalaeefar and Asgarian [18–21], and subsequently, a numerical behavioral model is proposed. Figure 1 shows the details of the proposed damper [18].

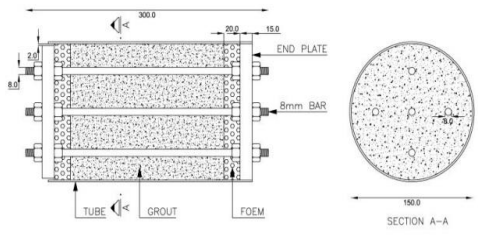

Fig. 1: Details of the Hybrid Axial Damper composed of the Steel and SMA Bars [18]

As can be seen, this damper consists of three main parts:

1- End plates: These plates are sufficiently thick to be considered rigid and thus only participate in carrying the axial load.

2- Bars connected to the end plates: These bars are selected from two types of materials, namely structural steel and shape-memory alloy (SMA). Steel bars are mainly responsible for dissipating seismic energy through plastic deformation, and the SMA bars contribute to returning the damper to its initial undeformed configuration (self-centering). Although SMA bars also dissipate a portion of the input energy, their primary role is recentering rather than energy dissipation. Furthermore, to prevent failure of the members near connections, a reduction in the section of the members has been developed. Hence, each bar is divided into two elastic and inelastic parts.

3- Confinement mechanism: For optimal use of the damper in compression and tension, the bars are confined with grout mortar. This confinement prevents buckling under compression, and as a result, the damper exhibits similar behavior in both tension and compression.

2.2 Modeling Process

The behavior of the members of this damper is very similar to that of the BRBs. On the other hand, the experimental studies by Tsai and Huang in 2002 [22] showed that BRBs can be simplified as a set of springs connected in series (Figure 2). Based on this analogy, each bar of the hybrid damper is numerically represented by an equivalent spring system.

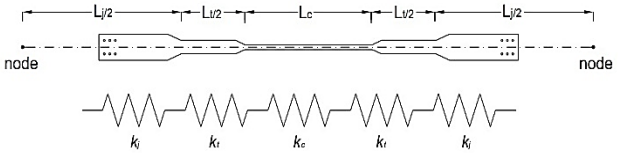

Fig. 2: Representation of the BRBs using Series Springs

Their studies confirmed that a BRB could be replaced by a spring with an effective stiffness of Ke.
The effective stiffness of the equivalent spring is defined based on the following relation:

$$K_e = \sum \frac{1}{K_i} = \frac{EA_jA_cA_t}{A_jA_tL_c+2A_cA_tL_j+2A_cA_jL_t} \qquad (1)$$

Due to the aforementioned points and also the similar behavior of the bars used in the damper with that of the BRBs, each steel and SMA bar in the hybrid damper is numerically replaced by a set of series springs (Figures 3 and 4).

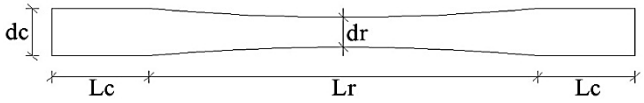

Fig. 3: Details of the Bars in the axial damper

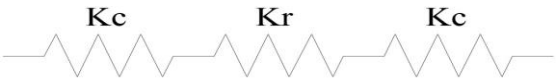

Fig. 4: Simplifying the bars with series springs

where:

L_r: length of the inelastic part of the bar

L_c: half of the elastic length of the bar

d_r: diameter of the inelastic part of the bar

d_r: diameter of the elastic part of the bar

Therefore, each bar is replaced by a spring with stiffness Ke, which is determined by the following equation.

$$K_e = \sum \frac{1}{K_i} = \frac{1}{K_c} + \frac{1}{K_r} + \frac{1}{K_c} \qquad (2)$$

By replacing each spring with each bar in the damper, a set of springs is formed that is in parallel with each other (Figure 5).

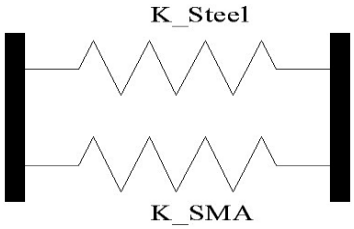

Fig. 5: Simplified model of the axial damper with a set of parallel springs

Accordingly, Equation (1) defines the effective stiffness of an individual bar, while the subsequent formulations extend this concept to represent the parallel assembly of bars and the overall stiffness of the hybrid damper.

$$K_e = K\_SMA + K\_Steel \qquad (3)$$

The numerical modeling framework developed in this section forms the basis for the parametric investigation presented in Section 3 and the behavioral model formulation described in Section 4.

2.3 Verification

After modeling, the accuracy of the program was evaluated by the experimental results of Asgarian and Jalaeefar [18]. For this purpose, the parameters of a damper consisting of two steel bars and two bars made of SMA, are introduced to the program (Table 1).

Table 1: Dimensions of the bar

Lc (Cm)	Lr (Cm)	dc (Cm)	dr (Cm)
1.5	6	0.8	0.5

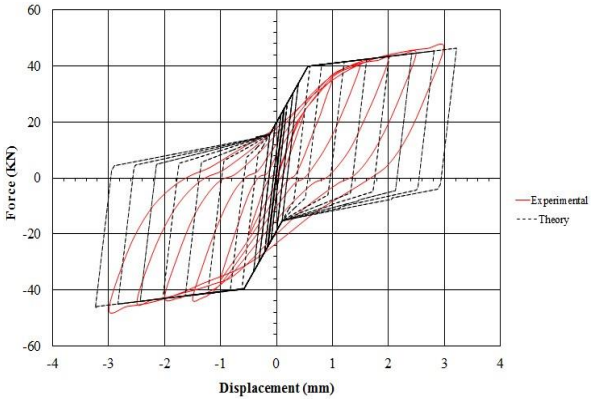

Fig. 6: Results of verification with actual values of elastic modulus

As shown in Figure 6, the maximum values of the forces are in agreement, but the slope of the two graphs, which indicates the stiffness of the damper, is different. On the other hand, the members of this damper are under axial load and the stiffness of the axial members is determined by the relationship $K = \frac{EA}{L}$. In this relation, E is the modulus of elasticity, A is the cross-section and L is the length of the member.

In short, the slope of the graphs depends on the geometry of the bars (cross-section and length) and their material (modulus of elasticity). The geometric parameters are the same in the experimental and theoretical models, so what causes this difference is the different values of the modulus of elasticity. The axial stiffness of the damper depends on both the geometry of the bars and the elastic modulus of the materials. Since the geometric parameters are identical in the numerical and experimental models, the observed difference in stiffness is attributed to the use of nominal elastic modulus values in the numerical model, whereas the experimental response reflects an effective elastic modulus influenced by material variability and testing conditions. By adopting an experimentally calibrated effective elastic modulus, the numerical model was updated, and the revised force–displacement response is shown in Figure 7, which has a good accuracy in estimating the maximum values of forces and their slope.

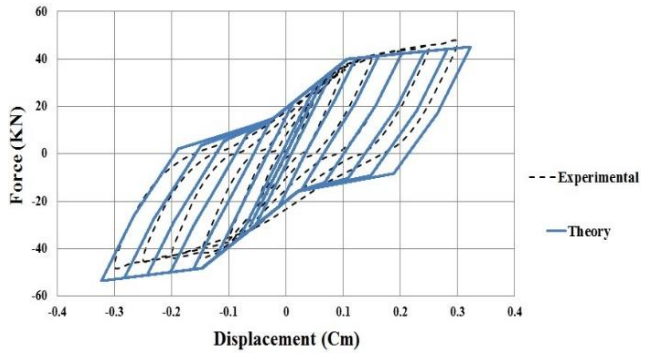

Fig. 7: Results of verification with modified values of elastic modulus

2.4 Material properties

To model the behavior of structural steel, a bilinear stress–strain relationship with isotropic hardening is adopted, assuming that its behavior in tension and compression is the same. The mechanical properties of the steel material are summarized in Table 2 using a standard numerical tabular format.

Table 2: Mechanical Properties of the Steel Material

Properties	Value
E_{Steel}	$2496910\,{}^{kg}/_{Cm^2}$
σ_y	$5075\,{}^{kg}/_{Cm^2}$
σ_u	$6622.5\,{}^{kg}/_{Cm^2}$

Moreover, the SMA has been simulated using six parameters as given in Table 3. The SMA material is modeled using a superelastic constitutive model defined by six parameters controlling elastic stiffness and phase transformation stresses.

Table 3: Mechanical Properties of the SMA

Properties	Value
E_{SMA}	$657000\,{}^{kg}/_{Cm^2}$
σ_s^{AS}	$5250\,{}^{kg}/_{Cm^2}$
σ_f^{AS}	$6250\,{}^{kg}/_{Cm^2}$
σ_s^{SA}	$3500\,{}^{kg}/_{Cm^2}$
σ_f^{SA}	$1000\,{}^{kg}/_{Cm^2}$
ε_L	3%

2.5 Loading Protocol

The specimens have been loaded according to the protocol recommended by SAC, which is illustrated in Figure 8 [23]. This cyclic displacement-controlled loading protocol was selected to ensure consistent evaluation of hysteretic behavior, energy dissipation capacity, and residual displacement across all parametric cases.

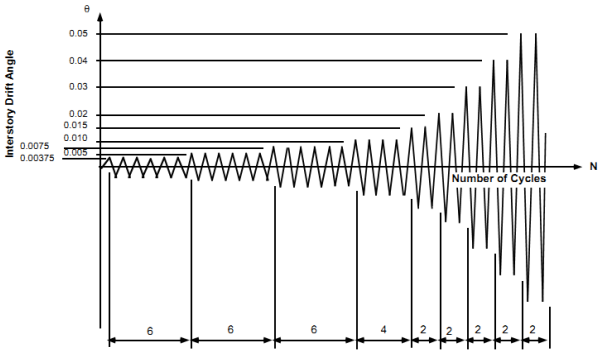

Fig. 8: SAC Loading Protocol

3. Results and Discussion

According to the numerical modeling framework described in Section 2, the influence of key geometric and material parameters on the cyclic behavior of the hybrid steel–SMA damper is investigated in this section. A base numerical model is first defined, and in each subsection, only one parameter is varied while all other parameters are kept constant.

3.1 Diameter of the Reduced Section

To investigate the effect of the diameter of the inelastic part on damper behavior, the diameter of the reduced section is varied for steel and SMA bars according to Table 4, while all other parameters are fixed at their base model values, by entering the SAC loading protocol, the results are extracted. The force-displacement curve is shown in Figure 9. Moreover, the dissipated energy versus the diameter of the bars is presented in Figure 10.

Table 4: Names of the Models based on change in diameter of the reduced section

Diameter of the reduced section (mm)	5	6	7	8
Changes of steel bar	DSteel5	Dsteel6	Dsteel7	Dsteel8
Changes of SMA bar	DSMA5	DSMA6	DSMA7	DSMA8

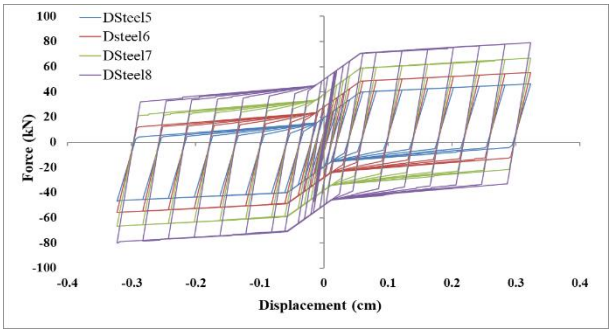

a) Steel bar

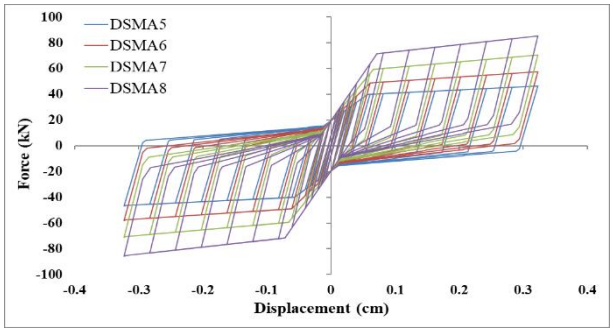

b) SMA bar

Fig. 9: Hysteretic Force-Displacement curve based on changes in diameter of the reduced section

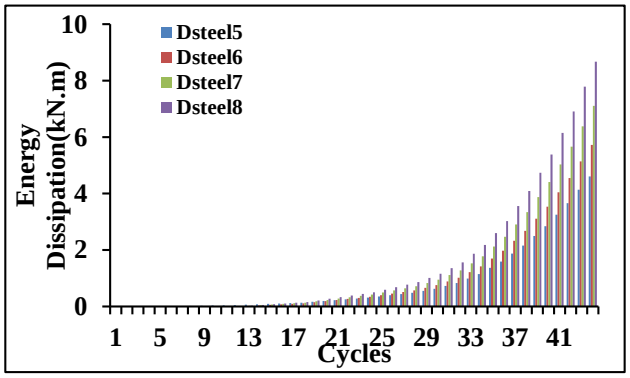

a) Steel bar

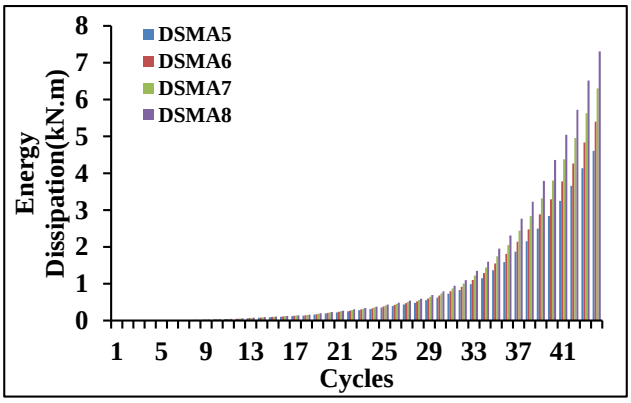

b) SMA bar

Fig. 10: Dissipated energy curve based on changes in diameter of the reduced section

The results indicate that increasing the diameter of the reduced section significantly increases the energy dissipation capacity and peak force of the damper. In particular, the cumulative energy dissipation at the end of the loading history increases from 4.61 kN·m for the DSteel5 model to 8.67 kN·m for the DSteel8 model, demonstrating the strong influence of the reduced-section diameter on damper performance. It also increases the damper force in each load cycle, so that increasing the diameter from 5 to 8 mm increases the force by 70% but has no effect on the reversibility of the damper. According to the above, it can be stated that increasing the diameter of the reduced steel part only improves the strength of the damper performance while having a negligible influence on residual displacement and self-centering capability.

Increasing the diameter of SMA bars significantly improves both energy dissipation and self-centering behavior, leading to a marked reduction in residual displacement. In contrast, increasing the diameter of steel bars has a limited effect on recentering, reducing residual displacement by only **8.8%**, compared to a **62%** reduction achieved by increasing the SMA bar diameter.

3.2 Number of bars

In this subsection, the influence of the number of steel and SMA bars on the damper response is examined, while all geometric and material properties of individual bars are kept constant. According to Table 5, the number of bars changes while other parameters are fixed.

Table 5: Name of Models based on the Number of Bars

Name	Number of steel bars	Number of SMA bars
DSt0	0	2
DSt2	2	2
DSt3	3	2
DSt7	7	2
DSMA0	2	0
DSMA2	2	2
DSMA3	2	3
DSMA7	2	7

The force-displacement curves of the bars after loading are obtained according to Figure 11. The energy absorption values from the hysteresis curves are also shown in Figure 12.

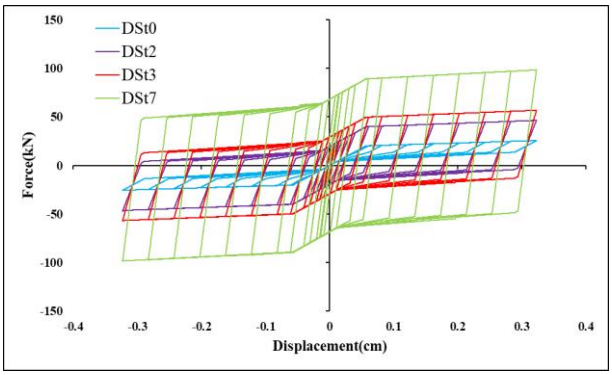

a) Steel bar

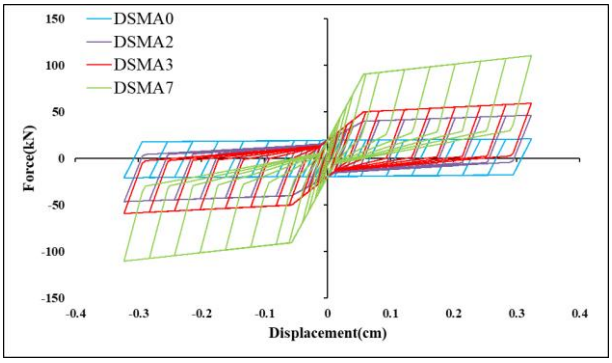

b) SMA bar

Fig. 11: Hysteretic Force-Displacement curve based on changes in the number of bars

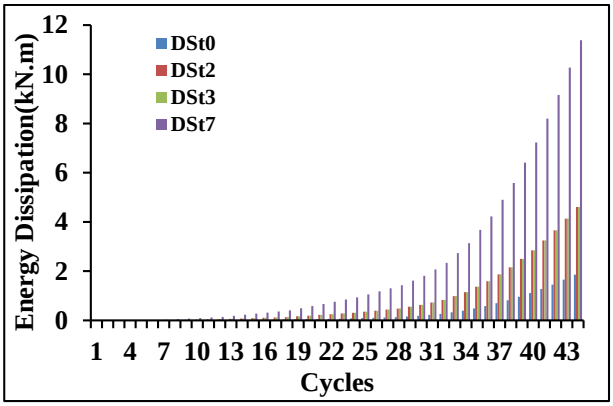

a) Changes in number of steel bars

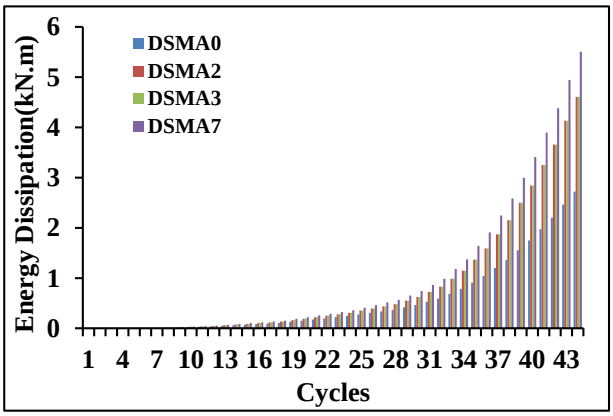

b) Changes in number of SMA bars

Fig. 12: cumulative dissipated energy curve based on changes in the number of bars

An increase in the number of steel bars significantly enhances energy dissipation and peak force. The cumulative dissipated energy increases from 1.86 kN·m (DSt0) to 11.38 kN·m (DSt7), while the peak force per cycle is approximately quadrupled. Also, increasing the number of steel bars has not had an effect on reducing the value of the residual displacement. As the number of SMA bars increases, the amount of cumulative energy dissipation and maximum force in the last load cycle in the DSMA0 specimen is 2.72 (kN.m) and 20.81 (kN) and in the DSMA7 specimen is 5.51 (kN.m), and (kN.m) is 36/101. Therefore, it is observed that the amount of energy loss and the maximum force increase the number of SMA bars increases. Regarding the performance of residual displacement, due to the suitable capabilities of SMA bars in self-centering, it decreases with increasing the number of bars and at the end of loading for DSMA0 damper is 3.08 mm and for the DSMA7 sample is equal to 0.92 mm. This indicates that the behavior of the damper in the dissipation of input energy is more affected by the number of steel bars. In terms of self-centering, increasing the number of steel and SMA bars leads to a decrease of 5.7% and 71.7% of residual displacements, respectively. It should be noted that although increasing the number of bars improves performance, practical geometric constraints and constructability

considerations limit the maximum feasible number of bars in real applications.

3.3 Length of the Reduced Section

In this subsection, the effect of the inelastic length of steel and SMA bars on damper behavior is investigated. These changes are made according to Table 6.

Table 6: Names of the Specimens based on length of the reduced part

Name	Bar length (cm)	Steel bar		SMA bar	
		Elastic (cm)	Inelastic (cm)	Elastic (cm)	Inelastic (cm)
EDSt,lr6	9	3	6	3	6
EDSt,lr12	15	3	12	9	6
EDSt,lr17	20	3	17	14	6
EDSt,lr22	25	3	22	19	6
EDSt,lr27	30	3	27	24	6
EDSMA,lr6	9	3	6	3	6
EDSMA,lr12	15	9	6	3	12
EDSMA,lr17	20	14	6	3	17
EDSMA,lr22	25	19	6	3	22
EDSMA,lr27	30	24	6	3	27

As mentioned, the SAC loading protocol is based on the yield displacement, and by changing it, the loading also varies. On the other hand, due to the similarity of the members of this damper with the BRBs, it is possible to determine the yield displacement from the following relationship:

$$U_y = \varepsilon_y l_r \quad (4)$$

Where $\varepsilon_y$and L_r are the yield strain and length of the reduced part, respectively.

On the other hand, the loading protocol used is based on the yield displacement. Therefore, to investigate the effect of inelastic length, the loading protocol should be changed and damping stress-strain diagrams are used for comparison in this case. Due to the above and due to the change along the reduced part, the loading protocol changes as shown in Figure 13.

According to the load difference entered in each specimen, in this section, stress-strain diagrams are used, which are presented in Figure 14. The curve of the amount of energy dissipation by changing the length of the inelastic part of the bars is also shown in Figure 15.

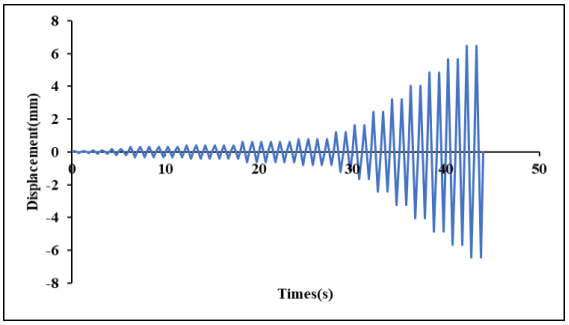

Specimen with Lr12

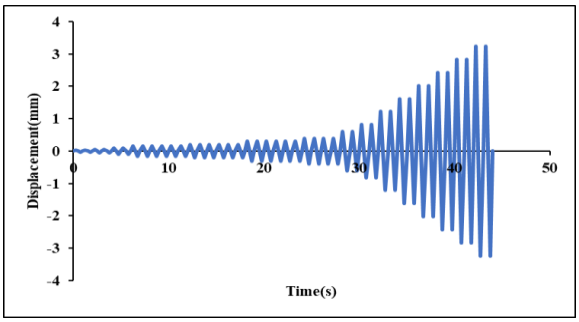

Specimen with Lr6

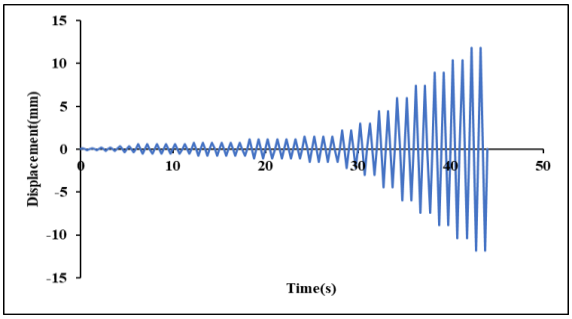

Specimen with Lr22

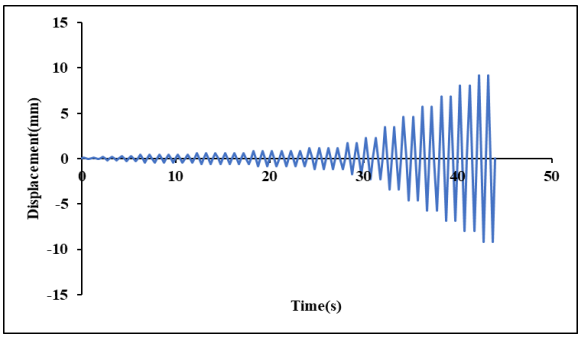

Specimen with Lr17

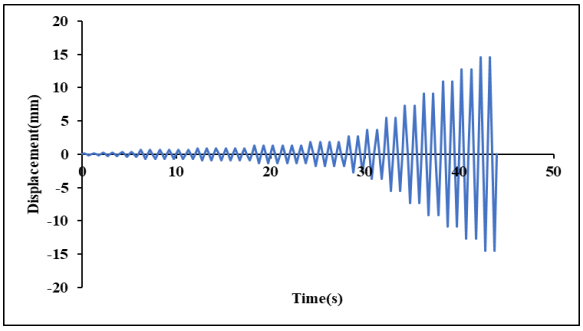

Specimen with Lr27

Fig. 13: Loading for each model

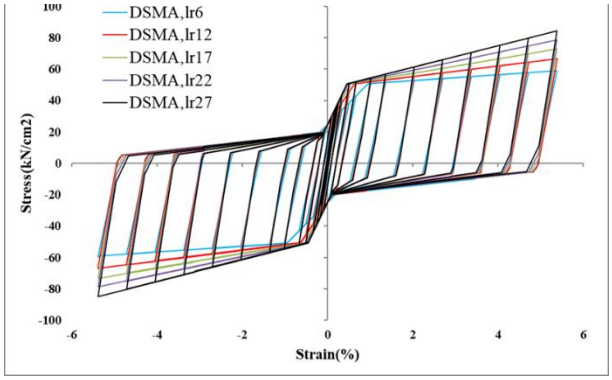

a) Length of the reduced part in the steel bar

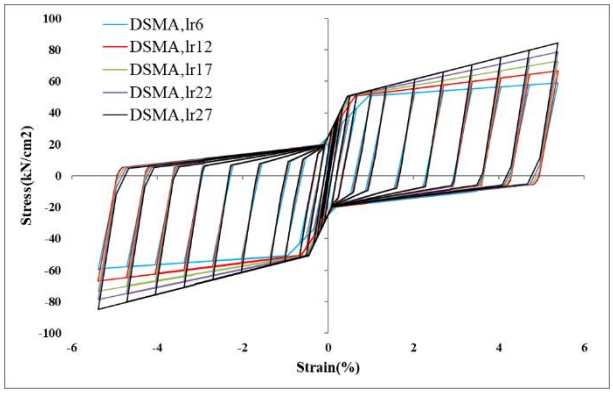

b) Length of the reduced part in the SMA bar

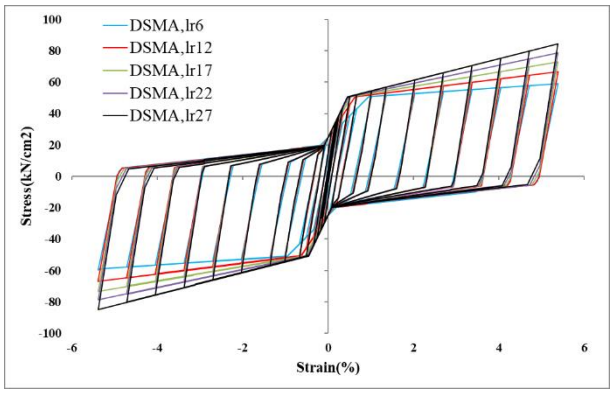

Fig. 14: stress-strain curve based on changes in length of the inelastic part

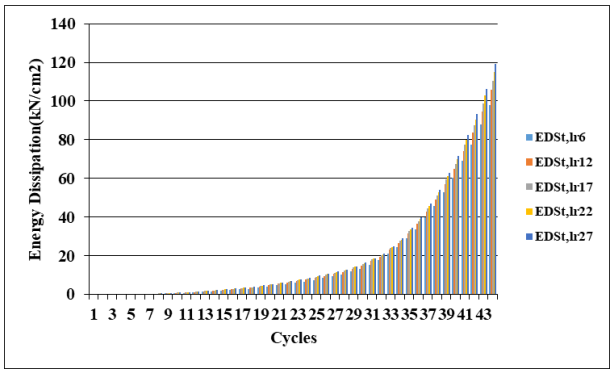

a) Length of the reduced part in the steel bar

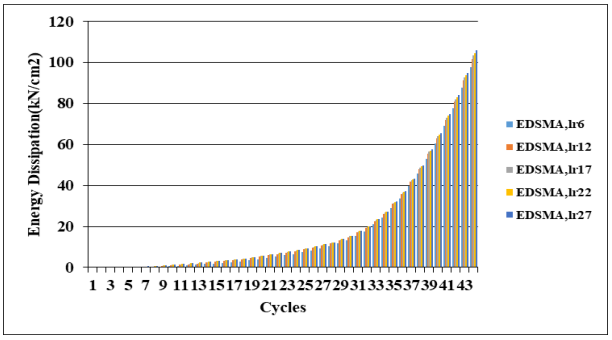

b) Length of the reduced part in the SMA bar

Fig. 15: cumulated dissipated energy based on changes in the length of the inelastic part

Increasing the inelastic length of steel bars results in higher energy dissipation and peak stress values from 97.751 (kN / cm2) to 119.085 (kN / cm2). Also, the amount of maximum force in each load cycle increases from 5934.034 (kN / cm2) to 84.445 (kN / cm2) and, as in the previous results, increasing the inelastic length has a small effect on the damper reversibility.

For SMA bars, increasing the inelastic length leads to only minor changes in energy dissipation and self-centering behavior, indicating that this parameter is less influential for SMA components. The values of dissipated energy and maximum force increase from 97.751 (kN / cm2) and 5934 (0334 kN / cm2) to 109.889 (kN / cm2) and 66.643 (kN / cm2), respectively. Also, increasing the length of the inelastic part of the SMA bar has a little effect on reducing the residual deformation rate. With the increase of the inelastic part of steel bars, the amount of energy dissipation has increased by 21.8%, while this amount is equal to 8.3% for SMA bars. As can be seen, the length of the inelastic part of the SMA bars has little effect on increasing the energy dissipation of the damper. The reduction rate of residual displacement is 10.3% in steel mode and 11.3% in SMA mode and has the same effect in both cases.

Overall, the inelastic length is a secondary parameter compared to diameter and number of bars, particularly for SMA elements.

3.4 Length of Elastic Part

The effect of the elastic length of steel and SMA bars is investigated by varying the elastic segment length while maintaining a constant inelastic length. In this case, the naming of the specimens is done according to Table 7. The force-displacement and energy dissipation curves are shown in Figures 16 and 17. It is worth noting that in this part of the modeling, the results of steel and SMA bars are the same.

Table 7: Details of the models for investigating the elastic length of the damper

Name	Bar length (cm)	Steel bar		SMA bar	
		Elastic (cm)	Inelastic (cm)	Elastic (cm)	Inelastic (cm)
ED,lc3	9	3	6	3	6
ED,lc9	15	9	6	9	6
ED,lc14	20	14	6	14	6
ED,lc19	25	19	6	19	6
ED,lc24	30	24	6	24	6

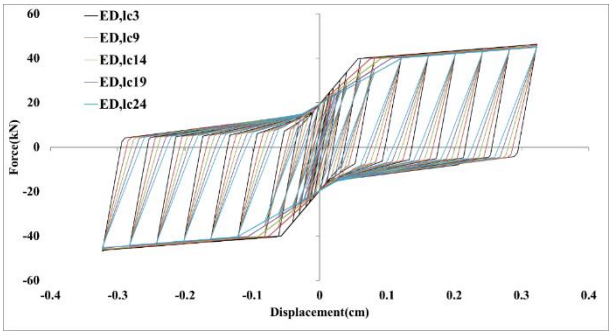

Fig. 16: Force-displacement curve of the damper based on changes in length of the elastic part

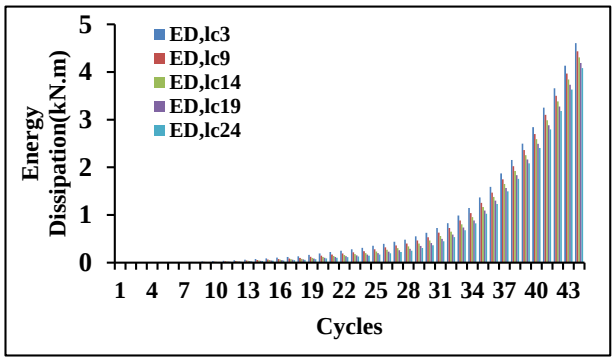

Fig. 17: Energy dissipation curve of the damper based on changes in the length of the elastic part

The results clearly indicate that increasing the elastic length reduces damper stiffness, peak force, and energy dissipation. For ED, lc3 and ED, lc24 models, the values of energy dissipation and maximum force in the last cycle are 4.607 (kN.m), 46.536 (kN) and 4.083 (kN.m), (kN), respectively. 45.098. The residual displacement decreases from 2.967 mm for the ED-3cc specimen to 2.681 mm, indicating that the influence of this parameter on self-centering behavior is minimal. As a result, with increasing the elastic part of steel and SMA bars, energy dissipation and residual displacement are reduced by 11.3% and 17.07%, respectively.

3.5 Steel Grade

The effect of steel grade on damper performance is examined by comparing conventional reinforcing steel (AIII) with low-yield-strength steel (EGS); however, the results indicate that modifying the steel grade does not consistently lead to improved overall damper performance. In some structures, in order to improve the behavior of the structure, it is necessary to use low-strength steels. Low-strength steels are abbreviated as EGS. The specifications of the steels are shown in Table 8. The characteristics of low-strength steel are extracted from the article by Saburi and Ziaei.

Table 8: Mechanical Properties of the Steel

Steel Type	Yield Strength (kg/cm2)	Yield Strain	Ultimate Strength (kg/cm2)	Ultimate Strain
AIII	5075	0.002032	6622.5	0.2
EGS	1200	0.0006	2500	0.45

By placing the specifications of the consumed steel, they are subjected to the same load, then their force-displacement diagrams are extracted. (Figure 18). Cumulative energy dissipation curves are also shown in Figure 19.

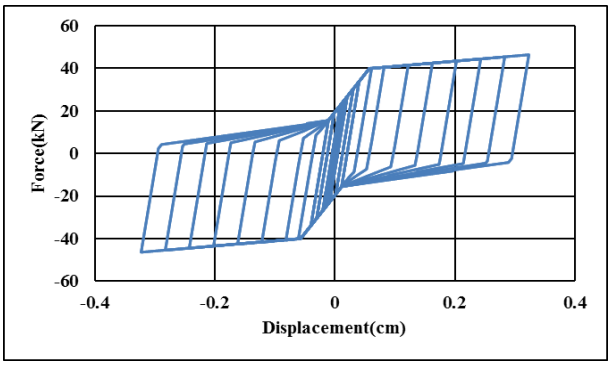

a) Damper DSt,AIII

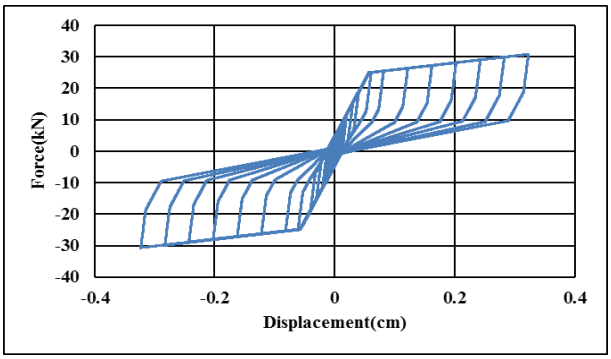

b) Damper DSt,EGS

Fig. 18: Force-displacement curve based on steel grade

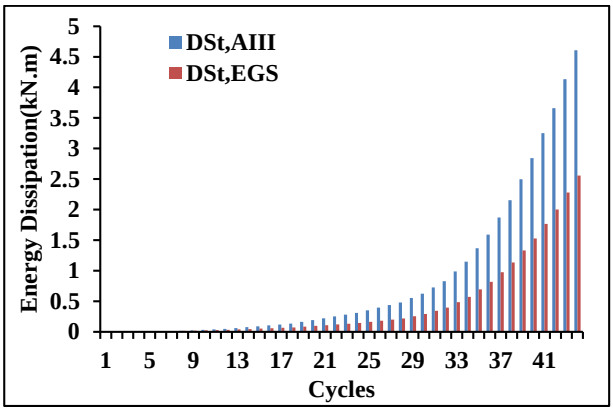

Fig. 19: Energy dissipation curve based on steel grade

The adoption of low-yield-strength steel significantly decreases the energy dissipation capacity and peak force of the damper, resulting in a 55.4% reduction in cumulative dissipated energy compared to conventional reinforcing steel. Also, the maximum force in each load cycle has decreased from 46.365 (kN) to 30.777 (kN). Regarding the amount of residual displacement, the use of mild steel leads to 87.5% reduction in the residual displacement. However, the residual displacement is significantly reduced, indicating improved self-centering behavior due to limited plastic deformation.

3.6 Comparative Effectiveness of Parameters

To compare the relative importance of the investigated parameters, their effects on energy dissipation, peak force, and residual displacement are summarized. The results indicate that:

- Diameter and number of steel bars are the most effective parameters for increasing energy dissipation.
- Number and diameter of SMA bars are the most influential parameters for improving self-centering behavior.
- Elastic length exhibits the least influence on overall damper performance.
- Steel grade governs the trade-off between energy dissipation and residual displacement.

This comparative assessment provides a quantitative justification for identifying the effective parameters used later in the development of the numerical behavioral model.

4. Numerical Behavioral Model

The purpose of this study is to determine a behavioral model for a hybrid damper which is done in this section. Based on the numerical parametric results presented in Section 3, this section introduces a numerical behavioral model capable of reproducing the hysteretic force–displacement response of the hybrid steel–SMA axial damper. The model formulation is directly informed by the observed effects of the key parameters identified in the parametric study and finally the accuracy of the model is evaluated by laboratory results.

The objective of this section is to develop a simplified yet accurate numerical representation of the nonlinear hysteretic behavior of the damper, suitable for implementation in numerical structural analyses.

4.1 General Description of the Behavioral Model

According to the obtained hysteresis diagrams, it can be seen that the force-displacement diagram of the damper is symmetrical under cyclic loadings. Therefore, the damper behavior is determined in one loading half-cycle and then its behavior is generalized to the next half-cycle.

This symmetry is attributed to the confinement of the bars and the identical behavior of the damper in tension and compression, as discussed in Section 2.

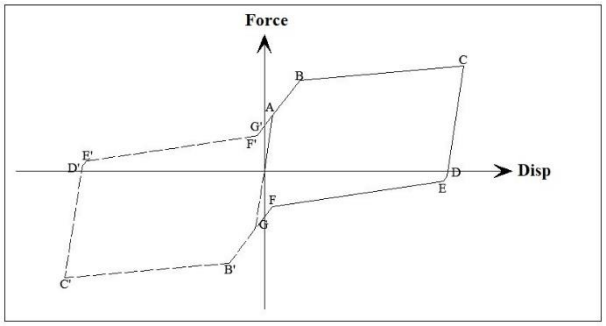

Fig. 20: Simplified force-displacement diagram of the damper

According to Figure 20, the force-displacement diagram of the damper in each half-cycle contains seven breaking points. These characteristic points are mirrored to the opposite half-cycle to represent the complete cyclic response of the damper.

Figure 21 shows the force-displacement diagram of steel and SMA bars. According to these diagrams, it can be concluded that the above points are in fact the breaking point of these diagrams. Therefore, by determining these points in each diagram, the desired seven points can be achieved.

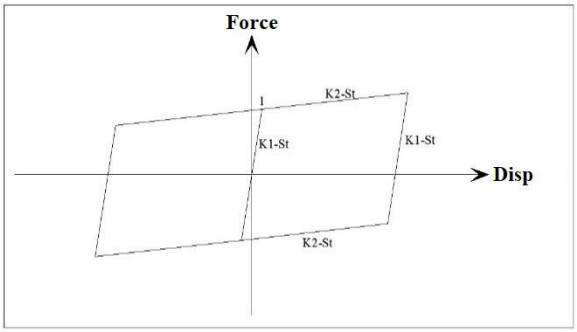

a) Steel components

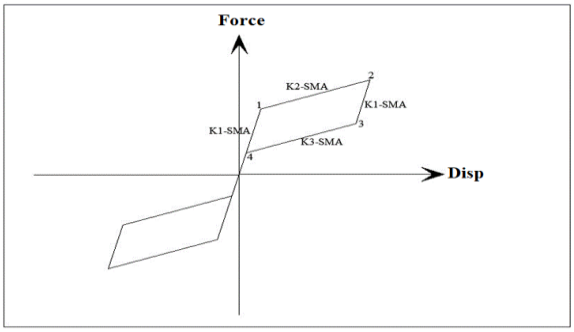

b) SMA components

Fig. 21: force-displacement diagram and stiffness distribution

Thus, the details of the force-displacement diagram of each damper component are calculated separately (stiffness and

breaking points), and the global damper response is obtained by assembling the steel and SMA component responses in parallel.

Determining the slope and breaking points on the force-displacement curve of the steel components

The elastic stiffness of the steel components and their corresponding breaking points are determined using Equations (5) and (6):

$$k_{1-St} = \frac{E_{St} A_{r-St} A_{c-St}}{A_{c-St} l_{r-St} + 2A_{r-St} l_{c-St}}$$
$$k_{2-St} = \frac{\alpha E_{St} A_{r-St} A_{c-St}}{A_{c-St} l_{r-St} + 2\alpha A_{r-St} l_{c-St}} \quad (5,6)$$

In the above equations:

E_{st} : Elastic Modulus of steel

$A_{r\text{-}St}$: area of the inelastic part of the steel component

$A_{c\text{-}St}$: area of the elastic part of the steel component

$L_{r\text{-}St}$: length of the inelastic part of the steel component

$L_{c\text{-}St}$: half-length of the elastic part of the steel component

α: post-yield coefficient

After determining the stiffness, the breaking point of the diagram must be determined (point 1). This is the point of yield displacement which is calculated as:

$$u_{yr-St} = \frac{p_{yr-St}}{k_{1-St}}$$
$$p_{yr-St} = A_{r-St} F_y \quad (7,8)$$

Where:

$U_{yr\text{-}st}$:yield displacement of the steel component

$P_{yr\text{-}St}$: yield force of the steel component

$K_{1\text{-}st}$: stiffness of the steel component before yielding

$A_{r\text{-}St}$:area of the inelastic part of the steel component

F_y: Yield strength of steel

Determining the slope and breaking points on the force-displacement curve of the SMA components

The stiffness of the SMA bars, corresponding to the slope of the force–displacement curve in different phases, is determined using Equations (9)–(11):

$$k_{1-SMA} = \frac{E_{SMA} A_{r-SMA} A_{c-SMA}}{A_{c-SMA} l_{r-SMA} + 2A_{r-SMA} l_{c-SMA}}$$
$$k_{2-SMA} = \frac{E_{SMA} E'_{SMA} A_{r-SMA} A_{c-SMA}}{E_{SMA} A_{c-SMA} l_{r-SMA} + 2E'_{SMA} A_{r-SMA} l_{c-SMA}}$$
$$k_{3-SMA} = \frac{p_{r-AS} - p_{r-AF}}{u_{r-AS} - u_{r-AF}} \quad (9\text{-}11)$$

In the above equations:

Elastic Modulus of SMA

Slope of the stress-strain curve between $\sigma_S^{AS}$and σ_F^{AS}

The force equivalent to σ_S^{SA}

The displacement equivalent to σ_S^{SA}

The force equivalent to σ_F^{SA}

The displacement equivalent to σ_F^{SA}

Area of the inelastic part of the SMA bar

Area of the elastic part of the SMA bar

Length of the inelastic part of the SMA bar

Half-length of the elastic part of the SMA bar

After determining the stiffness, the observed breaking points are determined as follows.

$$p_{r-MS} = A_{r-SMA} \sigma_S^{AS}$$
$$p_{r-MF} = A_{r-SMA} \sigma_F^{AS}$$
$$p_{r-AS} = A_{r-SMA} \sigma_S^{SA}$$
$$p_{r-AF} = A_{r-SMA} \sigma_F^{SA} \quad (12\text{-}15)$$

Equivalent forces of these points:

Where:

The force equivalent to σ_S^{AS}, point 1

The force equivalent to σ_F^{AS}, point 2

The force equivalent toσ_S^{SA}, point 3

The force equivalent to σ_F^{SA}, point 4

The Stress that initiates the conversion of austenite to martensite

The Stress that ends the conversion of austenite to martensite

The Stress that initiates the conversion of martensite to austenite

The Stress that ends the conversion of martensite to austenite

Displacement of the points equivalent to these points:

$$u_{r-MS} = \frac{p_{MS}}{k_{1-SMA}}$$
$$u_{r-MF} = u_{r-MS} + \frac{p_{r-MF} - p_{r-MS}}{k_{2-SMA}}$$

$$u_{r-AS} = u_{r-MF} - \frac{p_{r-MF} - p_{r-AS}}{k_{1-SMA}}$$
$$u_{r-AF} = \frac{p_{r-AF}}{k_{1-SMA}} \quad (16\text{- }19)$$

Where:

The displacement equivalent to σ_S^{AS}

The displacement equivalent to σ_F^{AS}

The displacement equivalent to σ_S^{SA}

The displacement equivalent to σ_F^{SA}

4.2 Representing the damper behavioral model

After determining the characteristic (breaking) points defined in Section 4-1, the numerical behavioral model illustrated in Figure 22 is proposed for the hybrid steel–SMA damper. Figure 22: Proposed numerical behavioral model of the hybrid damper.

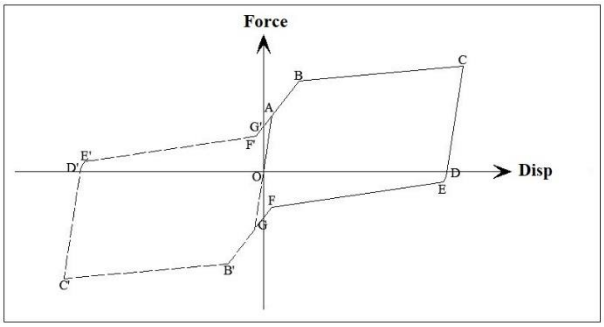

Fig. 22: The Proposed Behavioral Model

The force–displacement relationships are formulated for one loading half-cycle and subsequently generalized to the opposite half-cycle by exploiting the symmetry of the damper response. Therefore:

Point A represents the onset of yielding in the inelastic segment of the steel components. At this point, the damper response transitions from purely elastic to elastoplastic behavior.

$U_A = u_{yr-St}$

$$K_{OA} = N_{St}k_{1-St} + N_{SMA}k_{1-SMA} \quad (20\text{- }22)$$

$$P_A = K_{OA}U_A$$

Point B corresponds to the point at which the stress in the SMA bars reaches σ_S^{AS}initiating the forward phase transformation from austenite to martensite.

$\Delta u_B = u_{r-MS} - U_A$

$U_B = u_{r-MS}$

$$K_{AB} = N_{St}k_{2-St} + N_{SMA}k_{1-SMA} \quad (23\text{- }26)$$

$$P_B = K_{AB}\Delta u_B + P_A$$

Point C represents the completion of the forward phase transformation in the SMA bars, where the stress reaches σ_F^{AS}.

$\Delta u_C = u_{r-MF} - U_B$

$U_C = u_{r-MF}$

$$K_{CD} = N_{St}k_{2-St} + N_{SMA}k_{2-SMA} \quad (27\text{- }30)$$

$$P_C = K_{CD}\Delta u_C + P_B$$

To determine other points, the breaking point of the force-displacement diagram of the steel during loading must first be determined. This point is shown in Figure 23.

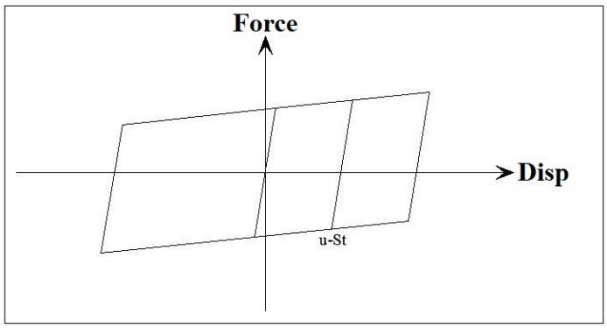

Fig. 23: Breaking location of the force-displacement curve of the steel components in unloading state

Therefore:

$$p_{St} = p_{yr-St} + k_{1-St}(U_C - u_{yr-St}) \quad (31)$$

$$u_{St} = \frac{k_{1-St}U_C - p_{St} + k_{2-St}u_{yr-St} - p_{yr-St}}{k_{1-St} - k_{2-St}} \quad (32)$$

The locations of Points D and E depend on the relative occurrence of steel yielding and SMA phase transformation during unloading. Accordingly, two possible cases are considered. To determine the location of D and E, the following cases occur:

Case 1 :

$if\ u_{st} \geq u_{r-AS}$

$\Delta u_D = u_{st} - U_C$

$U_D = u_{st}$

$$K_{CD} = N_{St}k_{1-St} + N_{SMA}k_{1-SMA} \quad (33\text{-}41)$$

$P_D = K_{CD}\Delta u_D + P_C$

$\Delta u_E = u_{r-AS} - U_D$

$U_E = u_{r-AS}$

$K_{DE} = N_{St}k_{2-St} + N_{SMA}k_{1-SMA}$

$P_E = K_{DE}U_E + P_D$

In this case, Point D corresponds to the breaking point of the steel force–displacement curve during unloading, while Point E represents the point at which reverse phase transformation initiates in the SMA bars, i.e., when the stress reaches σ_S^{SA}.

Case 2 :

$if\ u_{\text{r-AS}} \geq u_{St}$

$$\Delta u_D = u_{r-AS} - U_C$$
$$U_D = u_{r-AS} \quad (42\text{-}50)$$

$$K_{CD} = N_{St}k_{1-St} + N_{SMA}k_{1-SMA}$$
$$P_D = K_{CD}\Delta u_D + P_C$$
$$\Delta u_E = u_{St} - U_D$$
$$U_E = u_{St}$$
$$K_{DE} = N_{St}k_{1-St} + N_{SMA}k_{2-SMA}$$
$$P_E = K_{DE}\Delta u_E + P_D$$

In this case, Point D is defined as the point where the stress in the SMA bars reaches σ_S^{AS}whereas Point E corresponds to the breaking point of the steel force–displacement curve during unloading.

It should be noted that Points D and E are located close to each other during the initial loading cycles; however, as the imposed displacement amplitude increases, the distance between these two points becomes more pronounced.

Point F corresponds to the completion of the reverse phase transformation in the SMA bars, where the stress reaches σ_F^{SA}.

$$\Delta u_F = u_{r-AF} - U_E$$
$$U_F = u_{r-AF}$$

$$K_{EF} = N_{St}k_{2-St} + N_{SMA}k_{3-SMA} \quad (51\text{-}54)$$
$$P_F = K_{EF}\Delta u_F + P_E$$

Point G represents the unloading point at which the induced displacement of the damper returns to zero, completing the hysteretic cycle.

$$\Delta u_G = -u_{r-AF}$$
$$U_G = 0$$

$$K_{FG} = N_{St}k_{2-St} + N_{SMA}k_{1-SMA} \quad (55\text{-}58)$$

$$P_G = K_{FG}\Delta u_G + P_F$$

4.3 Unloading and Loading of the Behavioral Model

This section describes the numerical rules governing the loading and unloading paths of the proposed behavioral model based on the characteristic points defined in Sections 4-1 and 4-2. When loading, three modes occur for the damper:

Mode 1: Steel component remains elastic

In this case, in this mode, the steel components do not yield and both the SMA and Steel bars remain in their elastic state and loading and unloading takes place on the AA‘line with a KOA slope (Figure 24).

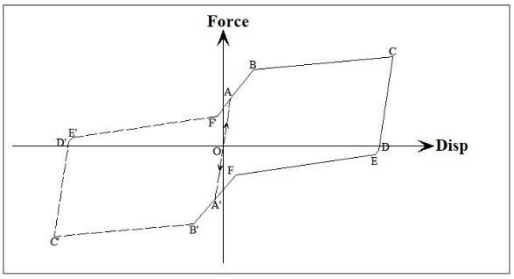

Fig. 24: Force-displacement curve before yielding of the steel bars

Mode 2: Steel component yields while SMA remains elastic. In this mode, the steel components yield after passing Point A, while the stress in the SMA bars remains below the transformation threshold σ_S^{AS}. Consequently, the SMA bars remain in the elastic regime. Therefore, the movement in the AB path is done with the slope of K_{AB}. Assume that the point is loaded at a point on the line AB, such as point h. In this case, the damper follows the h-i path. Point i is the point where the fracture occurs in the force-displacement diagram of the steel member. After reaching this point, the damper traverses the Gi path with a K_{FG} slope to zero the displacement of the damper. The loading and unloading paths corresponding to this mode are illustrated in Figure 25.

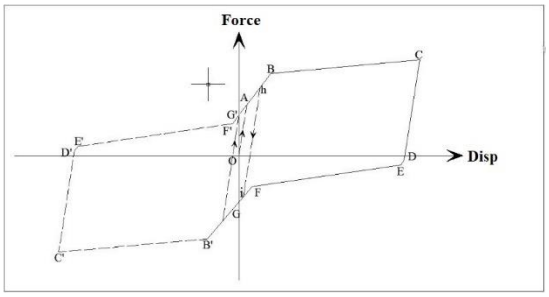

Fig. 25: Force-displacement curve after yielding of steel components and elastic state of SMA bars

Mode 3: Steel yields and SMA undergoes phase transformation

In this mode, both the steel and SMA bars enter nonlinear regimes after passing Point B, as the stress in the SMA bars exceeds the transformation initiation stress σ_S^{AS} . In this case, the steel and SMA bars enter their nonlinear phase after passing point B. Assume that loading occurs at point j in the BC path, in which case the damper travels the jm path with a slope of K_{DC}. After reaching point m, the slope of the graph changes and the path continues to point n with K_{DE}. Then the K_{EF} slope reaches point F and the K_{FG} slope becomes the zero shift at point G. The complete loading and unloading paths for this mode are illustrated in Figure 26.

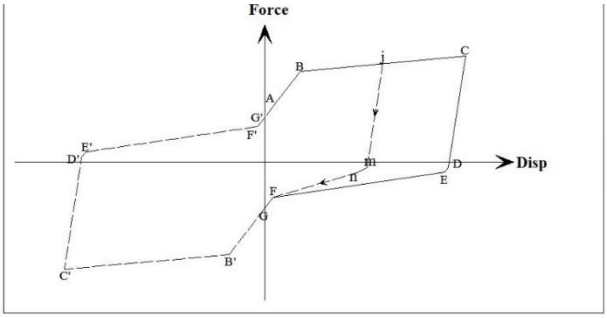

Fig. 26: Force-displacement curve after yielding of steel components and inelastic state of SMA bars

4.4 Verification of the Proposed Model

The accuracy of the proposed numerical behavioral model is verified using experimental results obtained from laboratory tests conducted on dampers composed of two steel bars and two SMA bars, as reported in [18]. Figure 27 presents a comparison between the experimental force–displacement response and the response predicted by the proposed model.

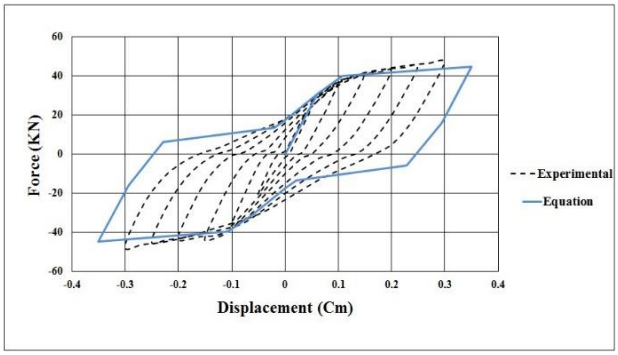

Fig. 27: Evaluation of the accuracy of the proposed behavioral model by laboratory results

As can be seen, the proposed behavioral model fits very well with the force-displacement diagram obtained from the experiment. The model is able to accurately reproduce the initial stiffness, yielding behavior, phase transformation plateau, unloading stiffness, and residual displacement observed in the experimental results. In addition, Figure 28 compares the force–displacement response obtained from the detailed numerical program described in Section 2 with that predicted by the simplified behavioral model. The close agreement between these two responses confirms that the proposed behavioral model can reliably represent the damper behavior while significantly reducing computational complexity.

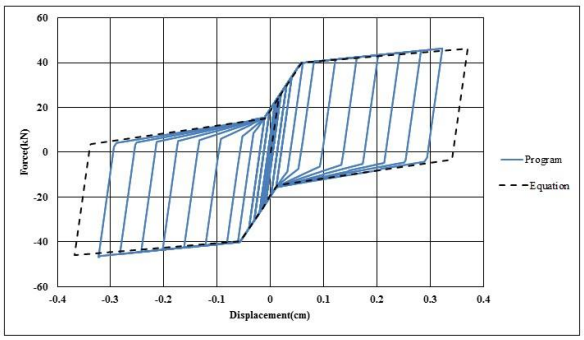

Fig. 28: Comparison between the Numerical and Experimental Force-Displacement Curves

5. Conclusion

In this paper, the influence of key geometric and material parameters on the cyclic behavior of a hybrid damper composed of steel and SMA bars was numerically investigated. In addition, based on the outcomes of the parametric study, a numerical behavioral model was developed to simulate the hysteretic response of the damper. The most notable conclusions are as follows:

- The parametric analyses demonstrated that the diameter of the inelastic part, length of the elastic part, length of the inelastic part, number of bars, and steel grade are the dominant parameters influencing the damper's force–displacement response, energy dissipation capacity, and residual displacement, as quantified in Section 3.
- Increasing the diameter of the inelastic part of the steel bars, enhances the energy dissipation capacity of the damper. However, it does not influence the returnability of the damper to its initial state. Moreover, as the diameter of the SMA bars increases, it is observed that the performance of the damper improves in terms of energy dissipation and self-centering capabilities. Although the energy dissipation contribution of SMA bars is lower than that of steel bars, increasing their diameter significantly enhances the self-centering performance and reduces residual displacement.
- It was observed that as the number of steel bars increases, energy dissipation of the damper improves considerably, although its self-centering capacity is not affected. Similarly, increasing the number of the SMA bars enhanced the energy dissipation capacity and more importantly, the self-centering capacity.

- Increasing the inelastic length of the steel bars leads to a noticeable increase in energy dissipation, whereas changes in the inelastic length of SMA bars showed a limited influence on both energy dissipation and self-centering capacity.
- Increasing the elastic length of the components, slightly reduced the energy dissipation capacity of the damper and did not affect the self-centering capability of the damper.
- The results indicate that selecting steel materials with excessively low yield strength does not necessarily improve damper performance, as reduced strength leads to lower energy dissipation. Therefore, an appropriate balance between strength and ductility is required in material selection.
- The SMA bars not only could return the damper to its initial state, but also played an important role in dissipating the seismic energy. Despite having a less significant role compared to the steel bars in this respect, they cannot be ignored.
- The proposed numerical behavioral model accurately represents the damper behavior under cyclic displacement-controlled loading conditions considered in this study.

In this model, seven characteristic points are required to simulate the hysteretic behavior of the damper. These points correspond to stiffness transitions, yielding, and phase transformation stages identified in the numerical force–displacement responses discussed in Sections 3 and 4.

References

[1] Rezaiee-Pajand, Mohaamad, and A. Baghban. "Controlling structures by inverse adaptive neuro fuzzy inference system and MR dampers." Numerical Methods in Civil Engineering 2.1 2017, 24-36.

[2] Mirtaheri, M., M. Salkhordeh, S. M. S Kolbadi, H. Mirzaeefard, and M. R. Razzaghian. "Evaluation of 2D concentrically braced frames with cylindrical dampers subjected to near-field earthquake ground motions." Numerical Methods in Civil Engineering 4, no. 3, 2020, 21-30.

[3] Kelly, J.M., Slinner, R.I. and Heine, A.J. Mechanisms of Energy Absorption in Special Devices for Use in Earthquake Resistant Structures, Bulletin of New Zealand National Society for Earthquake Engineering, 5(3). pp.63-88, 1972.

[4] Kelly, J.M., Slinner, R.I., and Heine, A.J. Hysteresis Dampers for Earthquake Resistant Structures, Earthquake Engineering and Structure Dynamic, pp. 287-296, 1975

[5] Andalib, Z., Kafi, M. A., Kheybardin, A., & Bazzaz, M. (2014). Experimental investigation of the ductility and performance of steel rings constructed from plates. Journal of Constructional steel research, 103, 77-88.

[6] Braconi,A.Morelli,F.Salvatore,W.“Seismic Protection of Structures Through an Innovative Steel- Based Self-Centering Hysteretic Device: Numerical Analysis and Tests” , 15 WCEE, Lisboa (2012)

[7] Motamedi, M., Hafezi, M., Yekrangnia., M. “Analytical Study of Steel Ring Connections as Hysteretic Metallic Damper”. 15 WCEE, 2012.

[8] X. T PENG, C. LIN, Y. M CAO, W. X DUAN, Seismic Behaviors of the Composite Central Brace with Steel Ring Damper, 7th International Conference on Energy and Environmental Protection (ICEEP 2018), 1089-1092.

[9] N. Gao, J. S. Jeon, D. E. Hodgson, R. DesRoches, An innovative seismic bracing system based on a superelastic shape memory alloy ring, Smart Materials and Structures. 25 (2016) 055030 (1-16 pp), doi:10.1088/0964-1726/25/5/055030.

[10] Z. Andalib, M. A. Kafi, M. Bazzaz, S. B. Momenzadeh, Numerical evaluation of ductility and energy absorption of steel rings constructed from plates, Engineering Structures 169 (2018) 94–106, https://doi.org/10.1016/j.engstruct.2018.05.034.

[11] X. Peng, C. Lin, Y. Cao, W. Duan, Nonlinear Finite Element Simulation on Seismic Behaviour of Steel Frame-Central Brace with Ring Damper, IOP Conf. Series: Materials Science and Engineering 472 (2019) 012031, doi:10.1088/1757-899X/472/1/012031.

[12] Darvishan, Ehsan. "Seismic Retrofit of Vulnerable Steel Frames Using Articulated Quadrilateral bracing system." Numerical Methods in Civil Engineering 4, no. 2 ,2019, 1-16.

[13] Zhu, S.Zhang, Y.” Seismic Behaviour of Self-Centering Braced Frame Buildings With Reusable Hysteretic Damping Brace”, Earthquake Engineering and Structural Dynamics, 1329-1346, 2007

[14] Karavasilis, T.Blackborough, T.Williams, M.”Development of nonlinear Analytical Model and Seismic Analyses of a Steel Frame With Self-Centering Devices and Viscoelastic Dampers”,Computers&Structures, Volume89, Issues 11–12, June 2011, Pages 1232-1240

[15] ozbulut, E.Hurlebaus, S.” Re-centering Variable Friction Device for Vibration Control of Structures Subjected to Near-Field Earthquakes”,Mechanical Systems and Signal Processing, Volume 25, Issue 8, November 2011, Pages 2849-2862.

[16] Qiu, C., Wang, H., Liu, J., Qi, J., & Wang, Y. (2020). Experimental tests and finite element simulations of a new SMA-steel damper. Smart Materials and Structures, 29(3), 035016.

[17] Mirzai, N. M., Cho, H. M., & Hu, J. W. (2021). Experimental study of new axial recentering dampers equipped with shape memory alloy plates. Structural Control and Health Monitoring, 28(3), e2680.

[18] Jalaeefar, A., & Asgarian, B. (2013). Experimental investigation of mechanical properties of nitinol, structural steel, and their hybrid component. Journal of Materials in civil Engineering, 25(10), 1498-1505.

[19] Jalaeefar, A., & Asgarian, B. (2014). A simple hybrid damping device with energy-dissipating and re-centering characteristics for special structures. The structural design of tall and special buildings, 23(7), 483-499.

[20] Jalaeefar, A., & Asgarian, B. (2021). Innovative hybrid damper with structural steel and nickel–titanium shape memory alloy bars. Proceedings of the Institution of Civil Engineers-Structures and Buildings, 174(8), 685-693.

[21] Asgarian, B., Jamalian, A., & Jalaeefar, A. (2021). Response Modification Factor of Steel Braced Frames Equipped with Smart Hybrid Re-Centering Device. International Journal of Steel Structures, 21(6), 2004-2017.

[22] Tsai, K. C., Hwang, Y. C., Weng, C. S., Shirai, T., & Nakamura, H. (2002, December). Experimental tests of large scale buckling restrained braces and frames. In Proceedings, Passive Control Symposium.

[23] Krawinkler, H., Gupta, A., Medina, R., & Luco, N. (2000). Loading histories for seismic performance testing of SMRF components and assemblies. SAC Joint Venture, Report no. SAC/BD-00/10. Richmond, CA.